International Journal of Research and Review
[Indexed, Peer-Reviewed Journal]
Volume 13; Issue: 2; February 2026
Website: www.ijrrjournal.com
Research Paper *E-ISSN: 2349-9788; P-ISSN: 2454-2237*

Synthesis and Characterization of TiO_2 Nanomaterials for Sustainable Photocatalytic Erythrosin B Dye Degradation

Tushar More[1], Sanjay Gadakh[2]

Department of Physics, KRT Arts BH Commerce & A M Science College, Nashik

Corresponding Author: Sanjay Gadakh

DOI: https://doi.org/10.52403/ijrr.20260233

ABSTRACT

In this work, we synthesised TiO_2 nanomaterials using the hydrothermal method. Confirmation of the nanomaterials was performed with several analytical techniques, including UV-DRS, FTIR, XRD, Raman, and SEM-EDX. The UV-Vis spectrum showed an absorption peak at 425 nm, corresponding to a band gap of 2.91 eV. FTIR analysis identified functional groups such as 415 cm^{-1} (Ti-O-Ti) and 1200 cm^{-1} (-OH). SEM-EDX confirmed a quasi-spherical morphology and the presence of Ti and O elements. XRD analysis determined an average crystallite size of 120 nm. The photocatalytic activity of the synthesised TiO_2 nanomaterials was assessed by degrading Erythrosin B (EB) dye under UV-visible light irradiation. The EB degradation rate reached 96.14% at 135 min, demonstrating excellent photocatalytic efficiency. The TiO_2 nanomaterials enhance separation efficiency and suppress electron-hole pair recombination. Thus, this work highlights the significant potential of nanomaterials to develop effective photocatalysts for the degradation of organic pollutants.

Keywords: Hydrothermal methods; TiO_2 nanomaterial; Erythrosin B; Photocatalytic degradation

INTRODUCTION

Environmental pollution, especially water contamination, has become a major global concern. Organic dyes, widely used across many industries, significantly contribute to aquatic pollution due to their toxicity and durability [1]. Conventional wastewater treatment methods often do not effectively eliminate these dyes. The adverse environmental and health impacts arising from the persistence of synthetic dyes, such as Erythrosin B (EB) (Fig. 1), when released into water systems and aquatic ecosystems, pose significant risks due to their toxicity, non-biodegradability, and persistence [2], [3]. Here are some emerging strategies to mitigate pollution through photocatalytic degradation, utilizing semiconductor nanomaterials. Although TiO_2 is a well-known photocatalyst, it has several limitations, including rapid electron-hole recombination and limited visible-light absorption [4], [5].

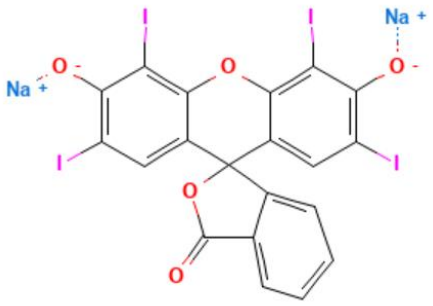

Fig. 1. Structure of Erythrosin B

Advanced oxidation processes, including photocatalysis, offer a potential solution to this serious problem. However, the low visible-light absorption of conventional photocatalysts, such as TiO_2, limits their practical application. Researchers have examined several methods to surmount this constraint, including doping with metal dopants and semiconductor hybridization [6]. The trapping of electrons by TiO_2 nanoparticles reduces the regeneration rate of electron-hole pairs, while the absorption range extends into the visible light region. Significant challenges arising from environmental pollution, as related to ecological integrity, health issues, or both, are generally caused by pollutants. Still, among these factors, the degradation of the aquatic environment emerges as a major contributor to health complications and the impairment of ecological balance [7], [8]. Organic dyes and pigments from various sectors pose significant threats to surface water due to their inherent toxicity, resistance to degradation, and aesthetic concerns. This paper highlights various conventional physicochemical wastewater treatment methods that are inefficient, costly, and associated with secondary emissions. Advanced oxidation has emerged lately as a high-potential technology for mitigating organic impurities. Of all these processes, photocatalysis can indeed be ranked among the most interesting, owing precisely to the possibility of harnessing solar power to accelerate chemical transformations. The process known as photocatalysis essentially involves producing reactive intermediates. Free radicals indeed represent their primary members. These radical $OH^{\cdot}$ can oxidize organically polluted impurities by transforming them into inorganic byproducts. TiO_2 is widely used as a significant semiconductor and photocatalyst, boasting outstanding photocatalytic properties. However, the large bandgap limits visible-light absorption, significantly reducing the overall photocatalytic efficacy. Several approaches have been employed to overcome these limitations, including metal doping, semiconductor coupling, and dye sensitization [9], [10], [11]. The nanoparticles can act as electron traps, thus lowering the regeneration rate of $e^{-}\ and\ h^{+}$ pairs and broadening the light absorption spectrum of TiO_2. The localized surface plasmon resonance effect due to nanoparticles not only increases light absorption further but also facilitates the generation of supplementary electrons that can participate in redox reactions. By evaluating these studies, we aim to demonstrate the improved performance, scalability, and potential of our TiO_2 nanomaterials in addressing current challenges in photocatalysis and related fields [12], [13], [14].

This work synthesised a highly efficient, environmentally friendly photocatalyst, TiO_2, using the hydrothermal method. The synthesised nanomaterial was analyzed using various analytical methods, including UV-Vis, FTIR, XRD, Raman, and SEM-EDX, to determine its structural and morphological properties. The photocatalytic efficiency of the nanomaterial was evaluated by monitoring the degradation of the EB dye under UV-visible light irradiation. Thus, this research contributes to the development of sustainable, practical approaches to addressing water pollution by elucidating the mechanisms underlying enhanced photocatalytic activity.

1. MATERIALS & METHODS

Metal precursors such as Titanium tetraisopropoxide $(Ti\{OCH(CH_3)_2\}_4, 284.2153\ g/mol)$ (TTP) (AR, ≥ 97 % purity) and Absolute ethanol (AR, ≥ 99.8 % purity) from Sigma-Aldrich and all AR-grade chemicals were used without further purification.

1.1. Methods

1.1.1. Synthesis of TiO_2 nanomaterials

In this method, we used a 2 M NaOH solution and added 3 mL of TTP to the solution, sonicated (60 ^{0}C and 2 h) and stirred vigorously. This solution was transferred to the autoclave for hydrothermal treatment at

140 °C for 12 h. After the hydrothermal treatment, the precipitate was filtered, washed, dried, and calcined at 350 ^{0}C for 4 h. Different analytical techniques were used to characterize the synthesised nanomaterials, including UV-Vis, FTIR, XRD, Raman, and SEM-EDX.

1.1.2. Photocatalytic EB dye degradation method

A model pollutant, EB, was utilized to evaluate the photocatalytic performance of the synthesized TiO_2 nanomaterial. The experiment used initial concentrations of 10^{-4} M for the EB dye and 250 mg per 100 mL for the TiO_2 nanomaterial. To account for any degradation due to adsorption of the reaction mixture containing EB and TiO_2, the mixture was kept in the dark for 10 min. The reaction mixture was irradiated under a photochemical reactor for up to 60 min. Absorbance spectra were recorded at intervals to track the kinetics of EB degradation. A reduction in dye concentration is indicated by a decrease in peak intensity at the characteristic wavelength of 526 nm. EB showed the least degradation in the absence of light, and the primary degradation pathway is photocatalytic. However, there was a marked decrease in the absorbance of the EB peak over time under the photochemical reactor. Thus, dye degradation was confirmed. We performed optimization of the dye degradation using some parameters like, ppm variation and catalyst dose.

To calculate the level of degradation, the standard formula was used to derive the percentage degradation of EB.

$$\textbf{\% of MB dye degradation} = \frac{[A]_0 - [A]}{[A]_0} \textbf{ x 100.}$$

Where $[A]_0$ = Initial absorbance of the EB dye solution at t = 0 min and [A] = Absorbance of the solution at t = t min.

2. RESULTS AND DISCUSSION

2.1. UV-DRS analysis

The optical performance of the materials was studied using UV-DRS to identify light absorption and bandgap energy. The absorption spectrum has a high-energy edge in the ultraviolet, with an absorption threshold of around 425 nm. The inset displays a Tauc plot, and $(\alpha hv)^{1/2}$ vs E yields a direct bandgap (Eg) of 2.91 eV (Fig. 2).

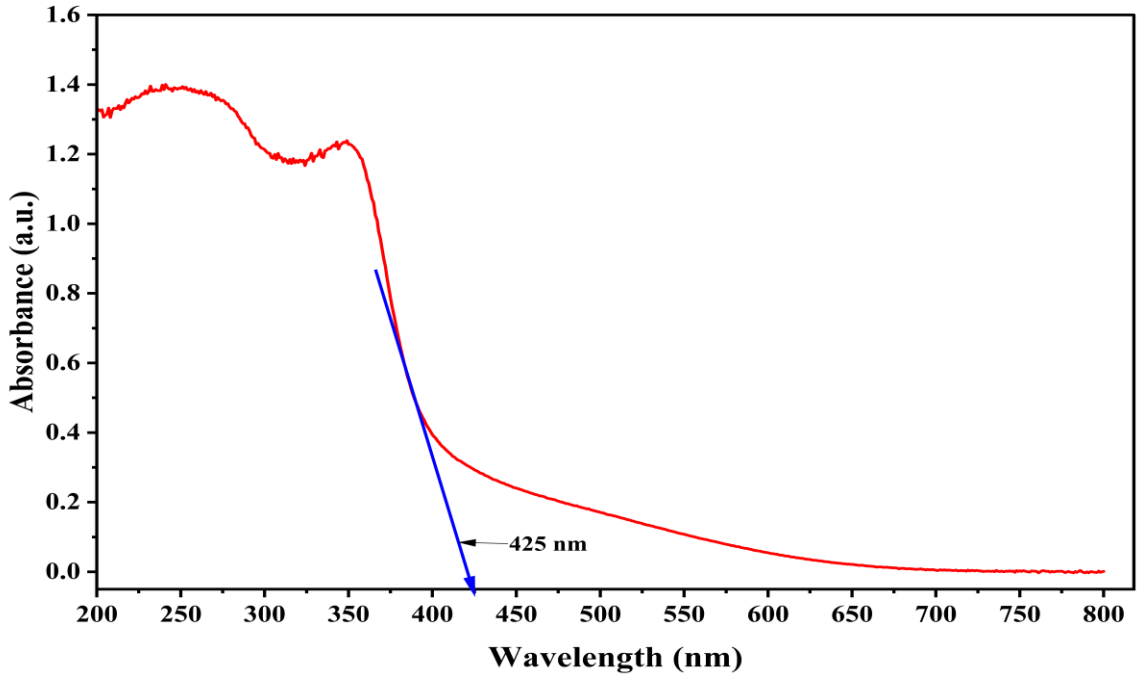

Fig. 2. UV-DRS spectra of TiO_2 nanomaterials

This number is in excellent agreement with the normal gap for TiO_2 (2.91 eV), which is lower than that of anatase (3.2 eV), making it easier to observe a little further into the near-visible energy spectrum [1], [15]. The bandgap energy (Eg) of the TiO_2 nanomaterial was calculated using the Tauc plot method. The Tauc equation for direct bandgap semiconductors is given by equation 1:

$$(\alpha hv)^{\frac{1}{n}} = A\left(hv - E_g\right) - - - -(1)$$

Where α is the absorption coefficient, hv is the photon energy, A is a constant, and n depends on the type of electronic transition (n = 2 for direct bandgap materials). The bandgap energy (E_g) was determined by extrapolating the linear region of the Tauc plot to $(\alpha hv)^{\frac{1}{n}} = 0$

The E_g value of the TiO_2 nanomaterial was obtained 2.91 eV [17]: (λmax = 400 nm)

This indicates that the nanomaterial may absorb visible light, as confirmed by its absorption spectrum, which shows a sharp peak in the visible region. A relatively high band gap energy would involve the highly energetic generation of e^- *and* h^+ Carrier pairs, upon photoexcitation, catalyse the degradation of organic pollutants.

2.2. XRD analysis

The XRD pattern (shown in Fig. for the TiO_2 nanomaterials) corroborates their well-crystalline nature. The most intense diffraction peak appears at 2theta = 27.4^0 and can be indexed to the (110) lattice plane of the Rutile phase (JCPDS No. 21-1276) [16]. The other characteristic peaks at 36.1^0, 41.2^0, 44.0^0, 54.3^0 and 56.6^0 are attributed to the (101), (111), (210), (211) and (220) planes, respectively (Fig. 3).

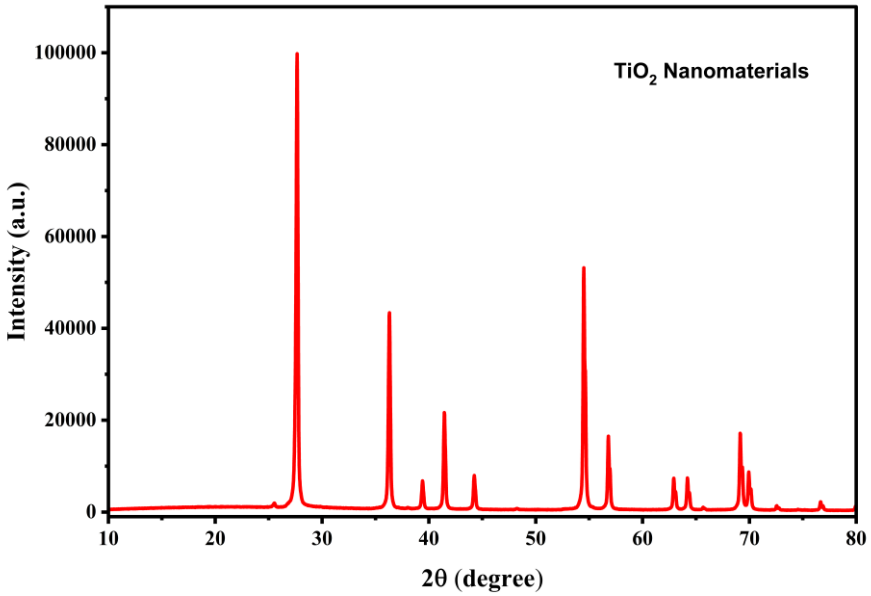

Fig. 3. XRD spectra of TiO_2 nanomaterials

The absence of the characteristic anatase peak at 25.3^0 confirms a phase-pure rutile sample. The sharp and high-intensity crystalline peaks indicate well-developed crystallinity and large crystallite sizes.

2.3. FTIR analysis

The FTIR spectra indicate chemical bonding and surface functional groups. The broad absorption band around 415 cm^{-1} can be assigned to the characteristic Ti-O-Ti stretching vibration, indicating the presence of an inorganic metal oxide network (Fig. 4).

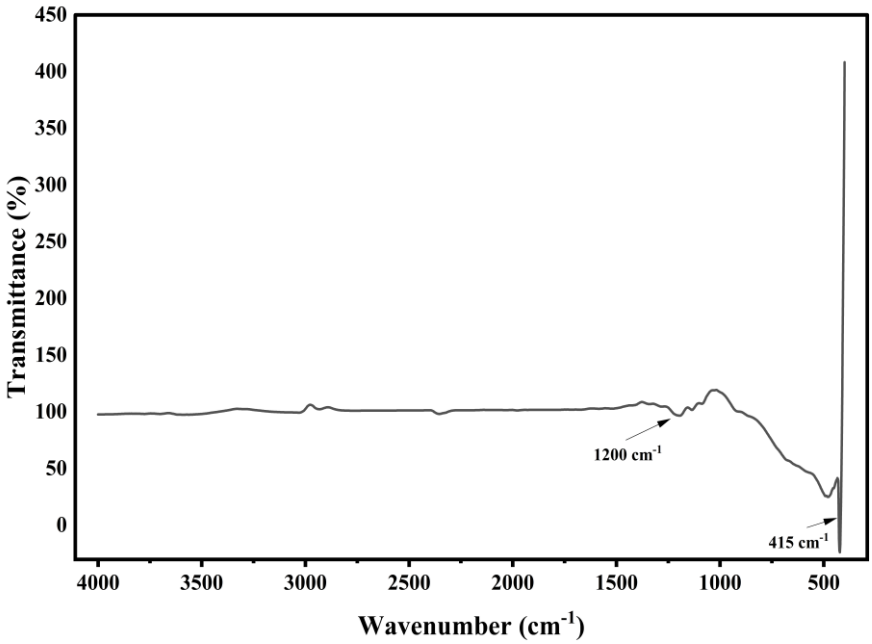

Fig. 4. FTIR spectra of TiO_2 nanomaterials

The smooth profile in the range of 150-4000 cm^{-1} indicates the absence of a large amount of surface-adsorbed water or hydroxyl (-OH) groups, usually typical for rutile form TiO_2 synthesised or treated at higher temperatures than the more hydrophilic anatase forms.

2.4. Raman Spectra

Raman spectra were used to study vibrational modes and phase purity of the synthesized TiO_2 nanomaterials. Three principal peaks are observed in the spectrum at 115 cm^{-1}, 468 cm^{-1}, and 612 cm^{-1}.

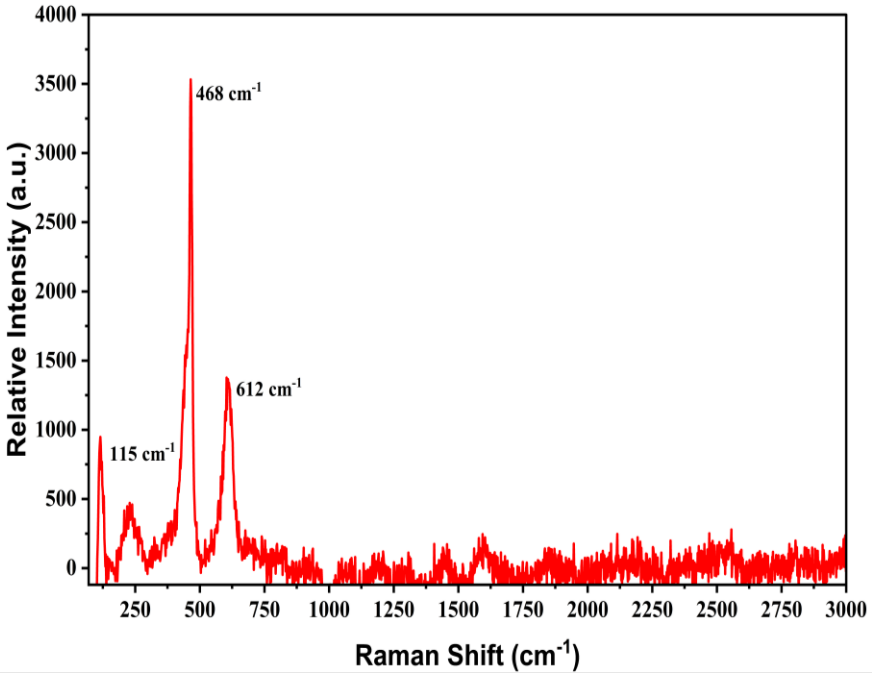

Fig. 5. Raman spectra of TiO_2 nanomaterials

These peaks are attributed to the B_{1g}, Eg, and A_{1g} vibrational modes of the rutile lattice. The Eg mode at 468 cm^{-1} and the A_{1g} mode at 612 cm^{-1} are the essential fingerprint

bands of rutile TiO_2. The sharp peaks' definition further supports the XRD results, indicating the construction of a well-ordered rutile skeleton.

2.5. SEM-EDX analysis

The SEM (Zeiss Sigma 500) image displays a heterogeneous surface with particles of different sizes and shapes clustered together. Both spherical and irregular forms are visible, likely representing TiO_2 particles. The nanomaterial appears rough and porous, which is beneficial for photocatalytic uses because it increases the surface area for light absorption and reactant adsorption [12], [19].

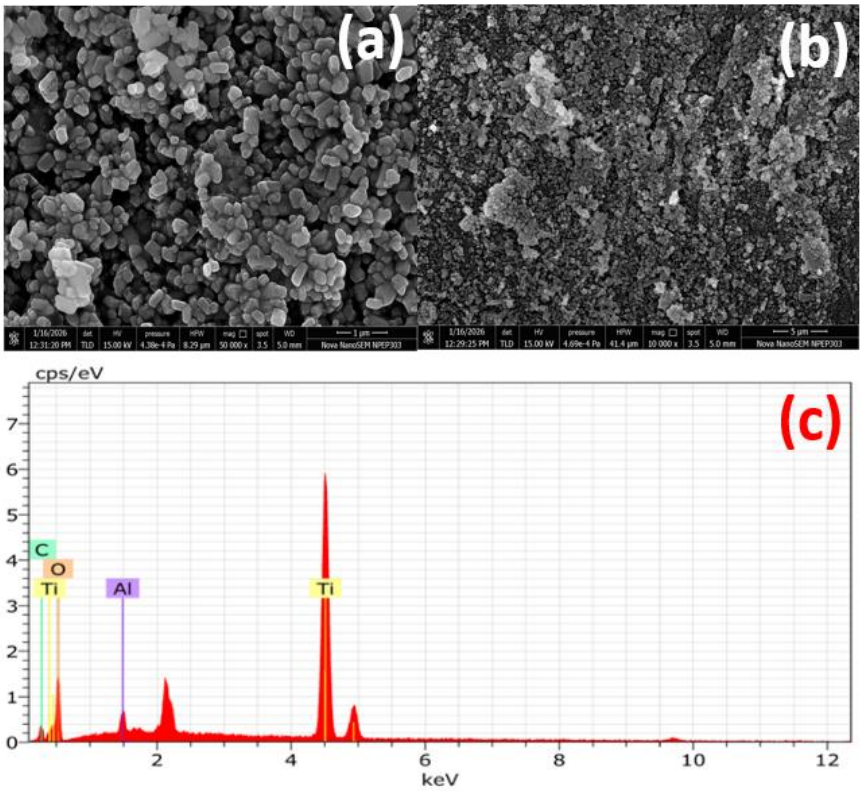

Fig. 6. SEM-EDX analysis of TiO_2 nanomaterials

EDX analysis confirmed an elemental composition of the synthesized TiO_2 nanomaterials (Table 1). The data obtained shows the presence of O and Ti elements in the main building blocks of the targeted materials.

Table 1. Elemental composition of the TiO_2 nanomaterials

El	AN	Series	unn. C [wt.%]	norm. C [wt.%]	Atom. C [at.%]	Error (1 Sigma) [wt.%]
Ti	22	K-series	51.46	66.42	39.82	1.55
O	8	K-series	23.26	30.02	53.86	4.14
C	6	K-series	1.48	1.91	4.56	0.49
Al	13	K-series	1.28	1.65	1.75	0.10
Au	79	M-series	0.00	0.00	0.00	0.00
		Total:	77.48	100.00	100.00	

Therefore, EDX analysis confirms the successful synthesis of the TiO_2 nanomaterials with the desired elemental composition. The presence of the Ti and O elements confirms the formation of TiO_2 nanoparticles within the nanomaterials. The elemental maps isolate Ti and O individually, with equal distribution within the sample, indicating the likely presence of TiO_2. Colour coding in elemental maps enhances the observed trend; yellow and orange colors dominate the expression of Ti and O. The observed distribution patterns align with the expected morphology of TiO_2 nanomaterials. The heterogeneous elemental distribution suggests that the synthesis process has yielded a well-dispersed composite, enabling intimate TiO_2 nanoparticles.

2.6. Photocatalytic dye degradation

The absorption spectra of EB dye degradation in the presence of TiO_2 nanomaterials at different dye concentrations are shown in Fig. 7.

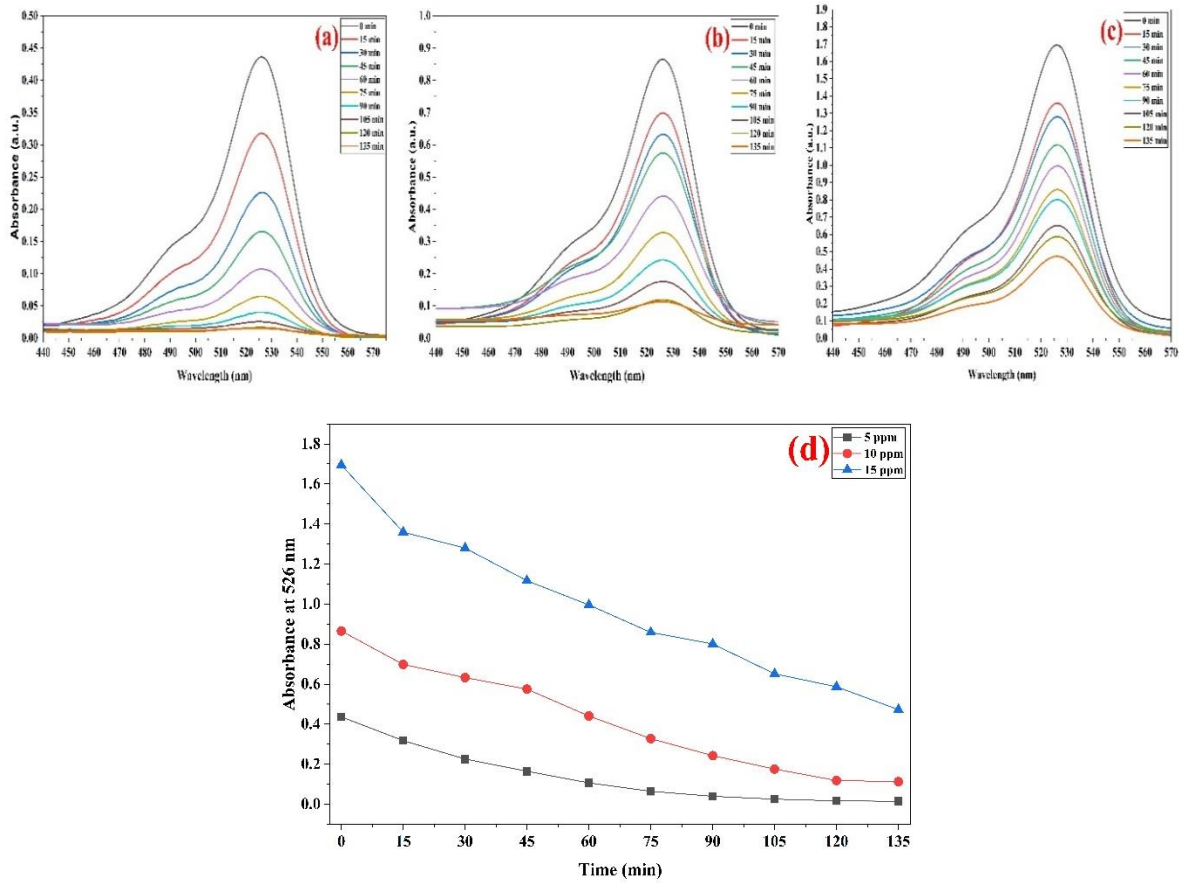

Fig. 7. Absorption spectra of EB dye degradation: a) 5 ppm, b) 10 ppm, c) 15 ppm, and d) Comparative absorption vs time (min) graph of EB dye degradation

The absorption spectra of EB dye degradation in the presence of TiO_2 nanomaterials at different catalyst doses are shown in Fig. 8.

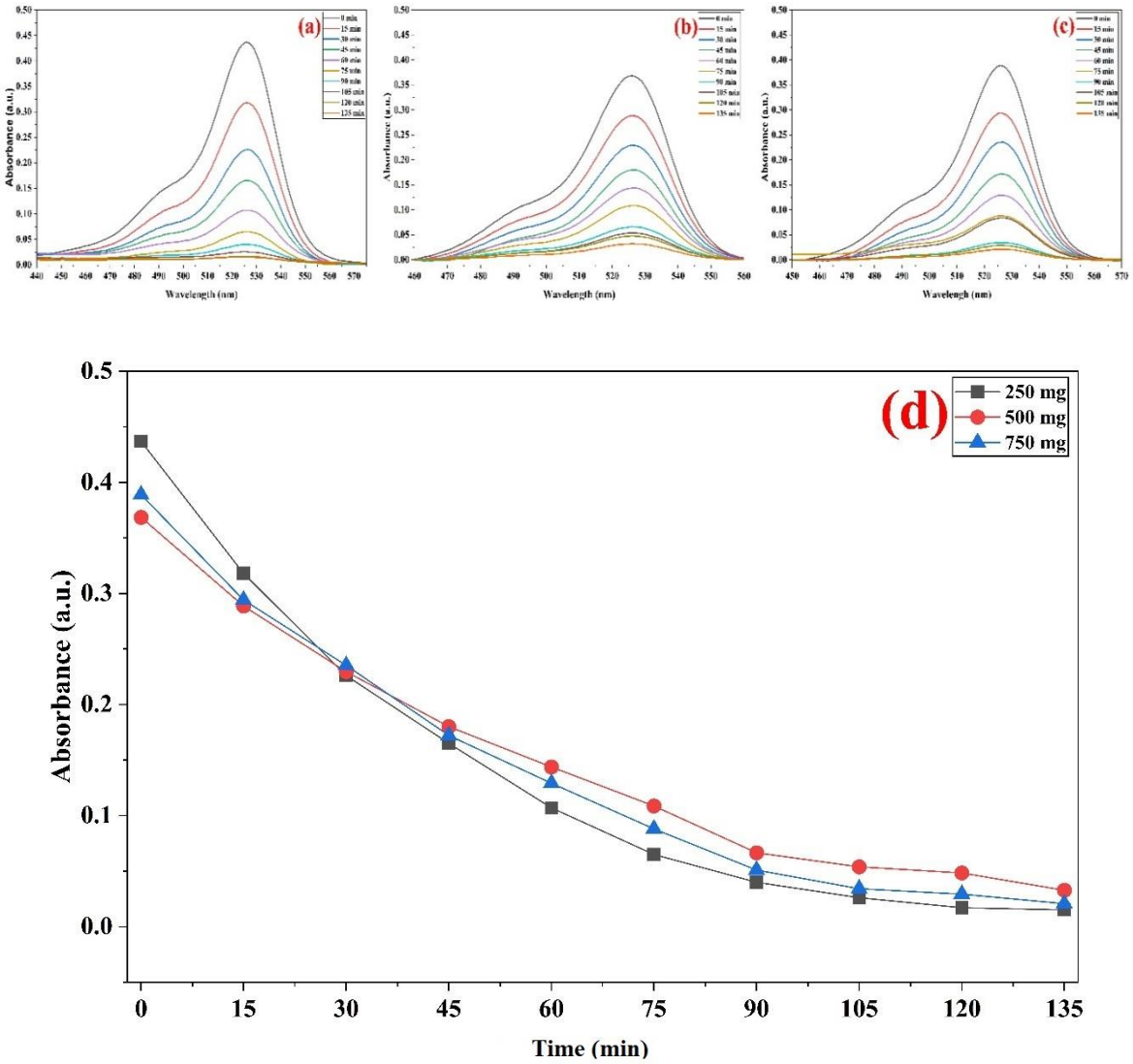

Fig. 8. Absorption spectra of EB dye degradation with different amounts of catalyst doses: a) 250 mg, b) 500 mg, c) 750 mg, and d) Comparative absorption vs time (min) graph of EB dye degradation

Table 2. Optimization of EB dye degradation in the presence of TiO_2 nanomaterials

Initial Concentration of EB dye (TiO_2=250 mg constant)	**Degradation (%)**	**Catalyst Variation (TiO_2) (initial dye concentration =5 ppm constant)**	**Degradation (%)**
5 ppm	96.43	250 mg	96.43
10 ppm	86.80	500 mg	91.11
15 ppm	72.16	750 mg	94.52

The mechanism of EB dye degradation in the presence of TiO_2 nanomaterials

a) ***Production of charge carriers [17]:***

=When the nanomaterials are TiO_2, they are subjected to enough illumination energy, and their results in the pair e- + h^+ from the support pair formation (Eq. 2) [20] (Fig. 14),

$$\boldsymbol{TiO_2 + hv\ (Vis) - - - \rightarrow TiO_2\ (h^+ + e^-) - - - - - - (2)}$$

An e^- and h^+ pair is formed from the excitation process, and an h^+ will be trapped within the VB.

b) ***Charge carriers trapping:***

Oxidation scavengers and electron holes combine and trap the h^+ and e^-, slowing

recombination down. Since the action of h^+ is directly related to the oxidation process of a dye or even towards the abstraction of hydrogen to yield water and an acceptor to form the acceptor $^{\cdot}OH$. Here, in schemes 1 and 2 (Eq. 3 and 4).

$$\textbf{Scheme 1: } H_2O + h^+ \longrightarrow OH^{\cdot} \quad (3)$$
$$\textbf{Scheme 2: } h^+ + OH^{\cdot} \longrightarrow OH^{\cdot} \quad (4)$$

An e^- acceptor must trap the e^- in the CB, so it cannot be recombined with the trapped hole. An e^- reduces O_2; the product formed is the reactive superoxide radical anions ($O_2^{\cdot-}$). This again generates more oxidizing species like H_2O_2. The reactions involved in generating supplemental hydroxyl radicals ($OH^{\cdot}$). Conversely, the electron that happens to be in the CB must be efficiently trapped by an electron acceptor not to be trapped by the fixed hole and, therefore, be recombined. During reduction, where O_2 takes up an electron, it forms reactive radical anions, namely, superoxide ($O_2^{\cdot-}$). This produces several other oxidizing agents, such as hydrogen peroxide (H_2O_2). The following are the reactions involved in the production of excess hydroxyl ($OH^{\cdot}$) radicals (Eq. 5 to 7):

$$O_2 + e^- \longrightarrow 2O_2^{-\cdot} + 2H^+ \longrightarrow HO_2^{\cdot} \quad (5)$$
$$H_2O_2 + e^- \longrightarrow OH^{\cdot} + OH^{\cdot} \quad (6)$$
$$H_2O_2 + O_2^{-\cdot} \longrightarrow OH^- + OH^{\cdot} + O_2 \quad (7)$$

c) ***Charge carriers' recombination:***
The process of regeneration of the e– & h+ pairs and that of trapped carriers can occur in the charge transfer mechanism in the process of exothermic heat release,

$$TiO_2(h^+ + e^-) \longrightarrow TiO_2 + heat \quad (8)$$

d) ***Photocatalytic degradation of dyes*****:**
The major photoreactions suggest that (e^- + h^+) pairs are included in the photocatalytic degradation of EB compounds. Highly reactive intermediates that continuously react with nearby species form $OH^{\cdot}$, O_2, HO_2, and photogenerated holes (h+) and eventually oxidize the entire structures of dyes. The mechanism describes how, in the degradation of dyes, the species OH., h+, and e- exercise their oxidative and reductive natures, as shown by schemes 1 and 3 (Eq. 9 to 11) [20], [21], [22].

$$Scheme\ 1: OH^{\cdot}\ or\ OH^- + EB \longrightarrow Degrade + Products \quad (9)$$
$$Scheme\ 2: H^{\cdot}\ or\ OH^{\cdot} + EB \longrightarrow Degrade + Products \quad (10)$$
$$Scheme\ 3: O_2^{-\cdot}\ or\ O_2^{\cdot} + EB \longrightarrow Degrade + Products \quad (11)$$

Photocatalytic degradation of EB dyes under sunlight irradiation using nanomaterials was monitored by absorbance measurements at various time intervals.

CONCLUSION

Here, we report the synthesis of TiO_2 nanomaterials via the hydrothermal method. The characterised nanomaterial was analysed using various analytical techniques, confirming its successful synthesis and inherent properties. The photocatalytic performance of the TiO_2 nanomaterial was systematically assessed by the degradation of EB dye under a photochemical reactor. The nanomaterial exhibited excellent photocatalytic activity, achieving a degradation rate of 96.14% within 135 min. Superior performances are associated with the materials, making charge separation more

efficient and reducing recombination e^{-} *and* h^{+} Pairs. The hydrothermal synthesis technique outlined here offers several benefits, including eco-friendliness, cost-effectiveness, and scalability. Consequently, this work highlights the significant potential in developing effective, environmentally benign agents for photocatalytic applications in environmental remediation [11], [21].

Declaration by Authors

Acknowledgement: None
Source of Funding: None
Conflict of Interest: No conflicts of interest declared.

REFERENCES

1. M. Rostami, A. Badiei, M. R. Ganjali, M. Rahimi-Nasrabadi, M. Naddafi, and H. Karimi-Maleh, "Nano-architectural design of TiO2 for high performance photocatalytic degradation of organic pollutant: A review," Environ. Res., vol. 212, p. 113347, Sep. 2022, doi: 10.1016/j.envres.2022.113347.
2. Y.-H. Chiu, T.-F. Chang, C.-Y. Chen, M. Sone, and Y.-J. Hsu, "Mechanistic Insights into Photodegradation of Organic Dyes Using Heterostructure Photocatalysts," Catalysts, vol. 9, no. 5, p. 430, May 2019, doi: 10.3390/catal9050430.
3. M. Kumar, V. P. Singh, S. B. Bhat, and R. Kumar, "Environmental risks of textile dyes and photocatalytic materials for sustainable treatment: current status and future directions," Discover Environment, vol. 3, no. 1, p. 132, Sep. 2025, doi: 10.1007/s44274-025-00337-0.
4. J. C. Mallia, A. A. Anastasi, and S. M. Briffa, "Developing Self-Cleaning Photocatalytic TiO2 Nanocomposite Coatings," International Journal of Surface Engineering and Interdisciplinary Materials Science, vol. 11, no. 1, pp. 1–20, Jun. 2023, doi: 10.4018/IJSEIMS.324757.
5. M. Yang, G. Liu, W. Zhao, F. Meng, Y. Lao, and Y. Liang, "Preparation and properties of TiO2 photocatalytic self—cleaning coating material for glass," International Journal of Low-Carbon Technologies, vol. 18, pp. 322–330, Feb. 2023, doi: 10.1093/ijlct/ctad015.
6. L. Yang, S. Luo, Q. Cai, and S. Yao, "A review on TiO2 nanotube arrays: Fabrication, properties, and sensing applications," Chinese Science Bulletin, vol. 55, no. 4–5, pp. 331–338, Feb. 2010, doi: 10.1007/s11434-009-0712-3.
7. E. Umar, M. Ikram, J. Haider, W. Nabgan, M. Imran, and G. Nazir, "A State-of-Art Review of the Metal Oxide-Based Nanomaterials Effect on Photocatalytic Degradation of Malachite Green Dyes and a Bibliometric Analysis," Global Challenges, vol. 7, no. 6, Jun. 2023, doi: 10.1002/gch2.202300001.
8. Jadhav, Vikram, Bhagare, Arun, Ali, Ismat H., Dhayagude, Akshay, Lokhande, Dnyaneshwar, Aher, Jayraj, Jameel, Mohammed, Dutta, Mycal, Role of Moringa oleifera on Green Synthesis of Metal/Metal Oxide Nanomaterials, Journal of Nanomaterials, 2022, 2147393, 10 pages, 2022. https://doi.org/10.1155/2022/2147393
9. S. Chang and W. Liu, "The roles of surface-doped metal ions (V, Mn, Fe, Cu, Ce, and W) in the interfacial behavior of TiO2 photocatalysts," Appl. Catal. B, vol. 156–157, pp. 466–475, Sep. 2014, doi: 10.1016/j.apcatb.2014.03.044.
10. D. Chen, Y. Wu, Z. Huang, and J. Chen, "A Novel Hybrid Point Defect of Oxygen Vacancy and Phosphorus Doping in TiO2 Anode for High-Performance Sodium Ion Capacitor," Nanomicro Lett., vol. 14, no. 1, p. 156, Dec. 2022, doi: 10.1007/s40820-022-00912-7.
11. S. H. Park, S.-J. Kim, S.-G. Seo, and S.-C. Jung, "Assessment of Microwave/UV/O3 in the Photo-Catalytic Degradation of Bromothymol Blue in Aqueous Nano TiO2 Particles Dispersions," Nanoscale Res. Lett., vol. 5, no. 10, pp. 1627–1632, Oct. 2010, doi: 10.1007/s11671-010-9686-y.
12. A. Kumar, V. K. Saxena, and R. Thangavel, "Self-cleaning properties of nanostructured TiO2 thin films synthesized via facile, cost-effective spin coating technique," 2019, p. 030319. doi: 10.1063/1.5113158.
13. D. John and V. S. Achari, "Graphene-based TiO2 photocatalysts for water decontamination: a brief overview of photocatalytic and antimicrobial performances," Curr. Sci., vol. 123, no. 9, p. 1089, Nov. 2022, doi: 10.18520/cs/v123/i9/1089-1100.
14. O. Landau and A. Rothschild, "Fibrous TiO2 gas sensors produced by electrospinning," J.

Electroceram., vol. 35, no. 1–4, pp. 148–159, Dec. 2015, doi: 10.1007/s10832-015-0007-9.
15. P. Ribao, J. Corredor, M. J. Rivero, and I. Ortiz, "Role of reactive oxygen species on the activity of noble metal-doped TiO2 photocatalysts," J. Hazard. Mater., vol. 372, pp. 45–51, Jun. 2019, doi: 10.1016/j.jhazmat.2018.05.026.
16. Y. MASUDA and K. KATO, "Synthesis and phase transformation of TiO2 nano-crystals in aqueous solutions," Journal of the Ceramic Society of Japan, vol. 117, no. 1363, pp. 373–376, 2009, doi: 10.2109/jcersj2.117.373.
17. V. R. Jadhav, J. S. Aher, A. M. Bhagare, A. C. Dhaygude, and D. D. Lokhande, "Plant-Mediated Green Synthesis of Nanoparticles for Photocatalytic Dye Degradation," in Phytonanotechnology, Singapore: Springer Nature Singapore, 2022, pp. 31–57. doi: 10.1007/978-981-19-4811-4_2.

How to cite this article: Tushar More, Sanjay Gadakh. Synthesis and Characterization of TiO2 nanomaterials for sustainable photocatalytic Erythrosin B dye degradation. *International Journal of Research and Review*. 2026; 13(2): 336-346. DOI: *10.52403/ijrr.20260233*

******